Experimental Test of the Greenberger–Horne–Zeilinger-type Paradoxes in and beyond Graph States

Zheng-Hao Liu,[1,2] Jie Zhou,[3] Hui-Xian Meng,[4,5] Mu Yang,[1,2] Qiang Li,[1,2] Yu Meng,[1,2] Hong-Yi Su,[6]
Jing-Ling Chen,[3,*] Kai Sun,[1,2] Jin-Shi Xu,[1,2,†] Chuan-Feng Li,[1,2,‡] and Guang-Can Guo[1,2]

[1]*CAS Key Laboratory of Quantum Information, University of Science
and Technology of China, Hefei 230026, People's Republic of China*
[2]*CAS Center For Excellence in Quantum Information and Quantum Physics,
University of Science and Technology of China, Hefei 230026, People's Republic of China*
[3]*Theoretical Physics Division, Chern Institute of Mathematics,
Nankai University, Tianjin 300071, People's Republic of China*
[4]*School of Control and Computer Engineering, North China Electric
Power University, Beijing 102206, People's Republic of China*
[5]*School of Mathematics and Physics, North China Electric Power University, Beijing 102206, People's Republic of China*
[6]*Graduate School of China Academy of Engineering Physics, Beijing 100193, People's Republic of China*
(Dated: May 3, 2021)

The Greenberger–Horne–Zeilinger (GHZ) paradox is an exquisite no-go theorem that shows the sharp contradiction between classical theory and quantum mechanics by ruling out any local realistic description of quantum theory. The investigation of GHZ-type paradoxes has been carried out in a variety of systems and led to fruitful discoveries. However, its range of applicability still remains unknown and a unified construction is yet to be discovered. In this work, we present a unified construction of GHZ-type paradoxes for graph states, and show that the existence of GHZ-type paradox is not limited to graph states. The results have important applications in quantum state verification for graph states, entanglement detection, and construction of GHZ-type steering paradox for mixed states. We perform a photonic experiment to test the GHZ-type paradoxes via measuring the success probability of their corresponding perfect Hardy-type paradoxes, and demonstrate the proposed applications. Our work deepens the comprehension of quantum paradoxes in quantum foundations, and may have applications in a broad spectrum of quantum information tasks.

I. INTRODUCTION

One of the most prominent features about quantum mechanics (QM) is its intrinsic nonlocality [1], namely, QM cannot be reconciled with local realism [2], thus no local-hidden-variable (LHV) models can completely reproduce the predictions of quantum theory. Since its discovery, quantum nonlocality has found many significant applications in quantum computation [3–5], device-independent quantum key distribution [6–8], and genuine random number generation [9, 10]. It is also a kind of resource playing a vital role in the field of quantum information [11, 12]. The Bell-type inequalities, which bound the correlations produced by any LHV models but can be statistically violated by QM, are arguably the most common tools for revealing the nonlocality. Some renowned examples include the two-qubit Clauser-Horne-Shimony-Holt inequality [13] and the multi-qubit Mermin-Ardehali-Belinskiĭ-Klyshko inequality [14–16].

Strikingly, in some measurement scenarios, QM and LHV models give contradictory predictions on whether a specific set of outcomes is even possible. Proofs of nonlocality stemmed from these scenarios are termed possibilistic nonlocality [17]. They occupy a strictly higher hierarchy than the statistical proof in the sheaf-theoretic approach, and can reveal the nonlocality of QM using very few measurements and copies of states prepared. The first proof of possibilistic nonlocality, due to Greenberger, Horne and Zeilinger (GHZ) [18], uses three qubits to formulate a paradox '$+1_\mathrm{C} = -1_\mathrm{Q}$' in every round of experiment. Here, the terminology $+1_\mathrm{C} = -1_\mathrm{Q}$ denotes the contradictory predictions given by the quantum and classical theory for the measurement outcome of an observable. Two-qubit systems can also manifest possibilistic nonlocality, but with a success probability of less than 1, and this way of observing nonlocality is later entitled Hardy's paradox [19]. Furthermore, Hardy's paradox has been generalized to the multi-setting scenarios [20], multipartite [21] and high-dimensional [22] systems.

The research of the GHZ paradox has achieved vigorous developments. It was experimentally tested [23] with three qubits, and can be observed in a fault-tolerant manner by using non-abelian anyons [24] to avoid the detection loophole. Besides the GHZ states, the earlier GHZ-type paradox is also known to be present in other pure states, such as the linear cluster states [25] and, more generally, a class of highly entangled multipartite states called graph states [26]. The investigation of the GHZ-type paradox has a continuous interest, since there are still some remnant issues with particular importance that require further investigation: (i) it is currently unknown whether a GHZ-type paradox can be exploited to determine a graph state; (ii) it is also not clear whether GHZ-

type paradoxes exist for the states that are not equivalent to graph states under local unitary; and (iii) there is no known method to experimentally test of a GHZ-type paradox with an efficient way, i.e, through its equivalent Hardy's paradox. Resolution to these issues may yield significant applications of quantum paradoxes.

In this article, we address the above issues to advance the study of GHZ-type paradoxes in quantum mechanics: First, a unified construction for the GHZ-type paradox is presented, naturally including all the previous results for graph states. For a graph with odd number of total vertices and at least one vertex being universal (i.e, connecting all the other vertices), observation of the GHZ-type paradox verifies the corresponding graph states, and efficiently detects multipartite entanglement. Second, due to a Hamiltonian description, some single-qubit Clifford equivalent graph states, their coherent superpositions and convex mixtures are also found to have the GHZ-type paradoxes. As such, the GHZ-type paradox exists *beyond* the graph states. Interestingly, for the convex mixtures of some single-qubit Clifford states that support the GHZ-type paradox $+1_c = -1_Q$ for Bell nonlocality, GHZ-type paradoxes $1_c = 2_Q$ for EPR steering [27] can be established, thus manifesting the sharp contradictions between a broader class of semiclassical models and quantum theory. Finally, the GHZ-type paradoxes can be converted to the *perfect* Hardy's paradox, on which we perform an experimental test through measuring the success probability in Hardy's paradox, thus providing an efficient way to reveal the GHZ-type paradoxes. Our experimental results are in agreement with the theoretical predictions with high accuracy, thus advance the study of the field of quantum paradoxes.

II. RESULTS

A. GHZ-type paradox for graph states

To introduce the idea of GHZ-type paradoxes, we begin with an explicit example based on the 3-qubit GHZ state $|GHZ_3\rangle = (|000\rangle + |111\rangle)/\sqrt{2}$. In this case, the results of the Pauli measurements,

$$
\begin{aligned}
[E_1 = \sigma_x^1 \sigma_x^2 \sigma_x^3] \, |GHZ_3\rangle &= +|GHZ_3\rangle, \\
[E_2 = \sigma_x^1 \sigma_y^2 \sigma_y^3] \, |GHZ_3\rangle &= -|GHZ_3\rangle, \\
[E_3 = \sigma_y^1 \sigma_x^2 \sigma_y^3] \, |GHZ_3\rangle &= -|GHZ_3\rangle, \\
[E_4 = \sigma_y^1 \sigma_y^2 \sigma_x^3] \, |GHZ_3\rangle &= -|GHZ_3\rangle,
\end{aligned}
\tag{1}
$$

cannot be interpreted by any LHV model: when we assign the dichotomic values $v = \pm 1$, as pre-determined by the hidden variables, to each measurement outcome, $\sigma_\nu^i \to v_\nu^i$, $\nu \in \{x, y, z\}$, $i \in \{1, 2, 3\}$, they must satisfy $v_x^1 v_x^2 v_x^3 = +1$, $v_x^1 v_y^2 v_y^3 = -1$, $v_y^1 v_x^2 v_y^3 = -1$, and $v_y^1 v_y^2 v_x^3 = -1$ in order to recover the predictions of QM. However, multiplying over these equations yields

$-1_Q \overset{\text{LHV}}{=} (v_x^1)^2 (v_y^1)^2 (v_x^2)^2 (v_y^2)^2 (v_x^3)^2 (v_y^3)^2 = +1_c$, a sharp contradiction.

The graph state is the common eigenstate of the stabilizing operators [28] for an undirected, connected graph $\mathcal{G}$, which has m vertices. We define C_i^j as the connectivity of the vertices i and j, so that $C_i^j = 1(0)$ means that vertices i and j are connected (disconnected). For each vertex i, the stabilizing operators read:

$$
S_i = \sigma_x^i \prod_{j \neq i} (\sigma_z^j)^{C_i^j},
\tag{2}
$$

where $i, j = 1, 2, \cdots, m$; $\sigma_{x,y,z}$ are Pauli matrices; and $(\sigma_z^j)^{C_i^j} = \sigma_z^j(\mathbb{1})$ if C_i^j is $1(0)$. The operators S_i are involutory and mutually commutative, and serve as the generators of an abelian group, namely, the stabilizing group. The ground state of the Hamiltonian $\mathcal{H} = -\sum_{i=1}^m S_i$ is then defined as the graph state $|G\rangle$ (i.e. $S_i|G\rangle = +|G\rangle$, $\forall i \in \{1, \cdots, m\}$). To construct the GHZ-type paradox, we focus on a vertex labelled as 1 with a degree of $n+1$, where $3 \leq n \leq m$. Without loss of generality, its neighbor vertices are labelled as $2, 3, \ldots, n$, and the other vertices unconnected to it are labelled $n+1, n+2, \ldots, m$. Then, the following theorem then holds.

$\{E\} :=$ (for odd n)	$\{(-1)^{a_i} S_1^{a_i} S_i S_{i+1} \,\|\, i \in \{2, \cdots, n-1\}\}$ $\cup \{S_1\} \cup \{S_1^{a_n} S_j \,\|\, j \in \{2, n\}\}$
$\{E\} :=$ (for even n)	$\{(-1)^{a_i} S_1^{a_i} S_i S_{i+1} \,\|\, i \in \{2, \cdots, n\}\}$ $\cup \{S_1\}$
Symbols definition	$a_i = 1 + C_2^n + \sum_{k=2, k \neq i}^{n-1} C_k^{k+1}$ $S_1^{a_i} = \begin{cases} S_1, & \text{if } \text{Mod}[a_i, 2] = 1, \\ \mathbb{1}, & \text{if } \text{Mod}[a_i, 2] = 0, \end{cases}$, $S_{n+1} = S_2$

Table 1. **Construction of GHZ-type paradoxes for graph states.** The set of observables $\{E\}$ as defined herein manifests a GHZ-type paradox for a graph state $|G\rangle$ with its graph representation $\mathcal{G}$ having connectivity C_i^j, and the stabilizing operators of $|G\rangle$ being S_i.

Theorem 1.— A GHZ-type paradox can be formulated from the observables E in Table. 1. The cardinality of $\{E\}$ is $n + 1$ when n is odd, and n when n is even.

A sketch of the construction of Theorem 1 is presented in the Methods section, and the detailed proof for it is provided in Supplementary Information (SI) [29]. In SI, we apply the Theorem 1 on all possible graphs with $m = 3$ and 4 to recover the GHZ-type paradoxes above and in [18, 25]. A concrete example for $m = 4$ is as follows.

Example 1.—Consider a $(m, n) = (4, 3)$ linear graph connected as 2—1—3—4. Its connectivity reads $C_1^2 = C_1^3 = C_3^4 = 1$, and the other C values are zero. The ground state of $\mathcal{H}$ is the 4-qubit cluster state with the form $|G\rangle = (|+0 + 0\rangle + |+0 - 1\rangle + |-1 - 0\rangle + |-1 + 1\rangle)/2$, where $|\pm\rangle = (|0\rangle \pm |1\rangle)/\sqrt{2}$. From theorem 1, we have $a_2 = a_3 = 1$, so the GHZ-type paradox can be derived from operators $\{S_1 = \sigma_x^1 \sigma_z^2 \sigma_z^3 \mathbb{1}, -S_1 S_2 S_3 =$
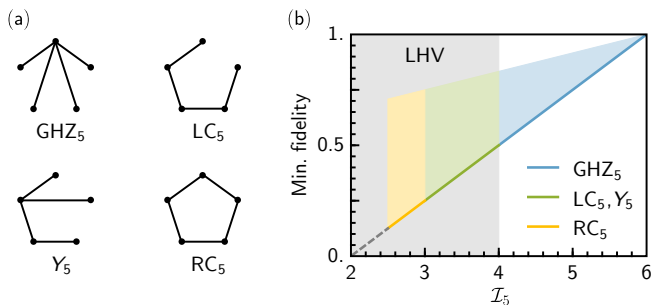
Fig. 1. **Five-qubit graph states and their verification.** There are four inequivalent 5-qubit graph states, namely, the GHZ states $|G_5\rangle$, the linear cluster state $|LC_5\rangle$, the Y state $|Y_5\rangle$ and the ring cluster state $|RC_5\rangle$. We derive the relation between the violation of the Bell's inequality $\mathcal{I}_5 \leq 4$ and the fidelity between the tested and target states. The colored region means at least two qubits are entangled, and a value exceeding the LHV bound reveals the genuine multipartite entanglement.

$\sigma_x^1\sigma_y^2\sigma_y^3\sigma_z^4, S_1S_2 = \sigma_y^1\sigma_y^2\sigma_z^3\mathbb{1}, S_1S_3 = \sigma_y^1\sigma_y^2\sigma_y^3\sigma_z^4\}$. Under local unitary transformation, the ground state is equivalent to the standard form of the cluster state $|LC_4\rangle = (|0000\rangle + |0011\rangle + |1100\rangle - |1111\rangle)/2$. Then we recover the usual construction of the GHZ-type paradox for the 4-qubit cluster state as [25]

$$
\begin{aligned}
[E_1 = \sigma_x^1\sigma_x^2\sigma_z^3\mathbb{1}] \quad & |LC_4\rangle = +\,|LC_4\rangle \,, \\
[E_2 = \sigma_x^1\sigma_y^2\sigma_y^3\sigma_x^4] \quad & |LC_4\rangle = +\,|LC_4\rangle \,, \\
[E_3 = \sigma_y^1\sigma_y^2\sigma_z^3\mathbb{1}] \quad & |LC_4\rangle = -\,|LC_4\rangle \,, \\
[E_4 = \sigma_y^1\sigma_x^2\sigma_y^3\sigma_x^4] \quad & |LC_4\rangle = +\,|LC_4\rangle \,.
\end{aligned}
\tag{3}
$$

Based on equation (3), we have the quantum prediction $\mathcal{Q} = \prod_{i=1}^{4}\langle LC_4|E_i|LC_4\rangle = -1$. However, in the LHV models, the product of the observable σ_ν^i's expectation values v_ν^i are $(v_x^1)^2(v_y^1)^2(v_x^2)^2(v_y^2)^2(v_y^3)^2(v_z^3)^2(v_x^4)^2 = +1$, thus leading to the GHZ-type paradox $+1_\mathrm{c} = -1_\mathrm{Q}$.

Quantum state verification.— A GHZ-type paradox is of particular interest if, using the specific observables, the paradox can be observed only with a specific graph state $|G\rangle$, similar to the situation of a Bell inequality that gives a single maximum for $|G\rangle$ [30–32]. From the form of Theorem 1, when $m = n$ is odd, any n operators E can still generate the n stabilizers of $\mathcal{G}$, so their grand total cannot have a degenerate ground state. Furthermore, in the case of $n = m$, there are no unmeasured qubits and the GHZ-type paradox constructed from operators E singles out $|G\rangle$.

Entanglement detection.—Theorem 1 also has a significant application in entanglement detection. In the case of odd n, we may transform the GHZ-type paradox into the Bell's inequality

$$
\mathcal{I}_n = \sum_{i=1}^{n+1} f_i\,\langle E_i\rangle \overset{\text{LHV}}{\leq} n-1 \,,
\tag{4}
$$

with $f_i = \langle G|E_i|G\rangle \in \{+1, -1\}$; the maximal violation is then directly given by $\mathcal{I}_n^{\mathrm{QM}} = n+1$. Note that every stabilizer appears an even number of times in all E, so $\prod_{i=1}^{n+1} f_i E_i = 1$. Moreover, the second-largest and the smallest eigenvalues of $\sum_{i=1}^{n+1} f_i E_i$ are $n-3$ and $-n-1$, respectively. According to the properties of the spectrum, the value of $\mathcal{I}_n$ evaluated for quantum state $|\psi\rangle$ can be related to the fidelity of $|\psi\rangle$ with respect to the target graph state. Using the two extremes above, it is straightforward to conclude that for relatively large $\mathcal{I}_n$, the fidelity is sandwiched between $(\mathcal{I}_n - n + 3)/4$ and $(\mathcal{I}_n + n + 1)/(2n+2)$. Therefore, the amount of violation of (4) gives a lower bound of the fidelity between an unknown state and the target graph state. Especially, violating (4) guarantees a fidelity of at least 50%.

Moreover, when the argument is applied to a target state with a large Schmidt measure [33], a quantum value $\mathcal{I}_n$ that is well below the LHV bound can still reflect non-trivial feature of entanglement. For example, the 5-qubit ring graph state $|RC_5\rangle$ in Fig. 1 has a Schmidt measure of 3, so a fidelity of $2^{-3} = 0.125$ with $|RC_5\rangle$ already guarantees entanglement. As this only requires achieving $\mathcal{I}_5 \geq 2.5$ with the Bell-type inequality (4), our construction has the notable feature of revealing non-classicality even when the observed correlation is not strong enough to reject the LHV models.

B. GHZ-type paradox beyond graph states

So far, only graph states have been known to be able to exhibit GHZ-type paradoxes. Here, we show that there are GHZ-type paradoxes presenting beyond graph states. Let us consider the measurement operators in Example 1. We can define a new Hamiltonian $\mathcal{H}' = -(E_1 + E_2 + E_4) + E_3$, whose ground states are interestingly two-fold degeneracies, i.e. $\mathcal{H}'|LC_4\rangle = -4\,|LC_4\rangle$ and $\mathcal{H}'|LC_4'\rangle = -4\,|LC_4'\rangle$, with $|LC_4'\rangle = (\mathbb{1} \otimes \mathbb{1} \otimes \mathbb{1} \otimes \sigma_x)|LC_4\rangle$. As in equation (3), we can verify that the extended cluster state

$$
|LC_4(\theta)\rangle = \cos\theta\,|LC_4\rangle + \sin\theta\,|LC_4'\rangle
\tag{5}
$$

also exhibits a GHZ-type paradox [29]. For $\theta \neq 0, \pi/2$, it is easy to check that the pure state $|LC_4(\theta)\rangle$ is not the common eigenstate of operators $\{S_i\}$; it thus cannot be viewed as a graph state. Therefore, we have a GHZ-type paradox for the non-graph state $|LC_4(\theta)\rangle$.

Furthermore, let us consider the following mixed state

$$
\rho(\theta) = \cos^2\theta|LC_4\rangle\langle LC_4| + \sin^2\theta|LC_4'\rangle\langle LC_4'|.
\tag{6}
$$

It can be verified that a GHZ-type paradox is also valid and that the paradox is θ-independent (i.e. $\mathcal{Q} = \prod_{i=1}^{4}\mathrm{tr}[\rho(\theta)E_i] = -1$). In addition, based on Fig. 1(c) in SI [29], we similarly obtain GHZ-type paradoxes for other non-graph states, i.e. the extended GHZ state $|GHZ_4(\theta)\rangle = \cos\theta\,|GHZ_4\rangle + \sin\theta\,|GHZ_4'\rangle$ and the mixed state $\rho'(\theta) = \cos^2\theta|GHZ_4\rangle\langle GHZ_4| +$

$\sin^2\theta|GHZ'_4\rangle\langle GHZ'_4|$, with $|GHZ_4\rangle = (|0000\rangle + |1111\rangle)/\sqrt{2}$ and $|GHZ'_4\rangle = (|1000\rangle + |0111\rangle)/\sqrt{2}$.

Steering paradox for mixed states.— In 2007, Wiseman *et al.* classified quantum nonlocality into three distinct types: quantum entanglement, EPR steering, and Bell's nonlocality [27]. EPR steering is a novel form of nonlocality that lies between entanglement and Bell's nonlocality. Gisin's theorem shows that for pure states, entanglement already indicates Bell nonlocality [34], so the relation among various types of non-classicality is subtler in mixed states. Here, we demonstrate that the GHZ-type proof is also applicable to EPR steering and, in particular, its scope is beyond the two-qubit pure state scenario [35].

For the mixed state in equation (6), an analogue GHZ-type paradox $1_C = 2_Q$ for EPR steering can be established, indicating a sharp contradiction between the local hidden-state (LHS) model and quantum theory. Concretely, when Alice prepares the state in equation (6), she keeps the first two qubits and sends the latter two qubits to Bob. Through EPR steering, Alice will persuade Bob that his two qubits do not have a LHS description, and therefore collapse to distinct conditional states according to Alice's measurement settings. Here, we demonstrate the case in which Alice's qubits subjects to two-settings measurements, namely, $\sigma_z \otimes \sigma_z$ and $\sigma_y \otimes \sigma_x$. According to the LHS model, the classical prediction for a steering parameter $\mathcal{I}_s$ is $\mathcal{I}_s^{\text{LHS}} = 1$, but quantum theory gives a prediction of $\mathcal{I}_s^{\text{QM}} = 2$, thus yielding the steering paradox $1_C = 2_Q$. The relevant details are given in SI [29].

C. GHZ-type paradoxes verified by Hardy-type paradoxes

To experimentally verify the GHZ-type paradox for nonlocality, conventionally the -1 factor between the quantum and classical predictions has to be demonstrated. For example, a direct way is to perform four successive measurements E_i's on the initial state $|LC_4\rangle$, and show, with the help of some interference techniques, that the final state is $e^{i\pi}|LC_4\rangle$. However, this way is not particularly amenable to experiment for the following reasons: (i) a highly pure initial state $|LC_4\rangle$ is required, and (ii) each measurement E_i acting on the state $|LC_4\rangle$ must be nondestructive. To circumvent these difficulties, we resort to other more effective approaches, which are related to measuring various probabilities. For instance, the GHZ-type paradox (3) can be converted to a perfect case of Hardy's paradox,

$$\begin{cases} P_1 = P(A_1^1 + A_2^1 + A_3^1 = 1) = 0, \\ P_2 = P(A_1^1 + A_2^2 + A_3^2 + A_4^1 = 1) = 0, \\ \dfrac{P_3 = P(A_1^2 + A_2^1 + A_3^2 + A_4^1 = 1) = 0,}{P_0 \equiv P_{\text{suc}} = P(A_1^2 + A_2^2 + A_3^1 = 1) \overset{\text{QM}}{=} 1 > 0,} \end{cases} \quad (7)$$

Here, the first three equations denote the Hardy-type constraints, and P_{suc} represents the success probability

for observing a LHV-impossible event. Equation (7) implies that a GHZ-type paradox can be viewed as a perfect Hardy's paradox, for which P_{suc} equals 1 in quantum mechanics [36]. The sharp contradiction $+1_C = -1_Q$ in the GHZ-type paradox is thus equivalent to $0_C = 1_Q$ in Hardy's paradox (where $P_{\text{suc}} = 0$ for LHV models and $P_{\text{suc}} = 1$ for quantum theory; see SI for further details about the conversion and measurement settings).

D. Experimental implementation

Using a photonic setup, we experimentally tested the GHZ-type paradoxes for some typical four-qubit graph and non-graph states via the perfect Hardy-type paradox. The steering paradox for the mixed state in equation (6) was also observed. The three unequivalent GHZ-type paradoxes for graph states with $m \leq 4$ were all tested in our experiment. Moreover, graph states with more qubits can be effectively generated in the linear optics setup by using, for example, the photon fusion gate [38], the polarizing beam splitter (PBS) gate [39] and the controlled-Z gate [40]. In SI, we give a recipe for generating all $m = 5$ graph states.

In this work, the four-qubit state was encoded using a two photons scheme [41, 42], with each photon's polarization and path degrees of freedom utilizing two logical qubits. Fig. 2(a) shows the quantum circuit for flexible state generation. Starting from a maximally entangled polarization qubit state of $|\Phi^+\rangle = (|00\rangle + |11\rangle)/\sqrt{2}$, we applied a controlled-NOT gate on two path qubits to obtain the GHZ state $|GHZ_4\rangle$. For cluster state $|LC_4\rangle$ generation, two Hadamard gates and a controlled-Z gate operating on the polarization qubits converted the state to $(|++00\rangle + |+-11\rangle)/\sqrt{2}$. We then projected the first two qubits of the input state onto $|00\rangle\langle 00| + |11\rangle\langle 11|$ basis to obliterate the different inputs on the polarization qubits. This process postselected the system wavefunction into the 4-qubit cluster state $|LC_4\rangle$. There is a 50% probability of conducting a successful postselection for such an input state. The final probabilistic gate was reminiscent of the PBS gate [39] in the linear optics system. When two photons meet at a PBS, only the superposition of wavefunction components with the same polarization results in coincident two-photon detection. Further generation of states $|LC_4(\theta)\rangle$ and $|GHZ_4(\theta)\rangle$ can be realized by performing transformation $\mathcal{R}(\theta) = \cos\theta + \sigma_x\sin\theta$ on one of the polarization qubits. This gate is non-unitary and probabilistic, as is common in the one-way quantum computation scenario.

The experimental setup is shown in Fig. 2(b). We exploited Hong-Ou-Mandel (HOM) interference [43] to certify the spatial and temporal overlap of the two photons at the PBS gate. As shown in the inset of Fig. 3, the visibility of the HOM dip was 97.1%, sufficient for observing the sharp Hardy-type paradox. Details about the setup and the HOM interference can be found in the Methods section.
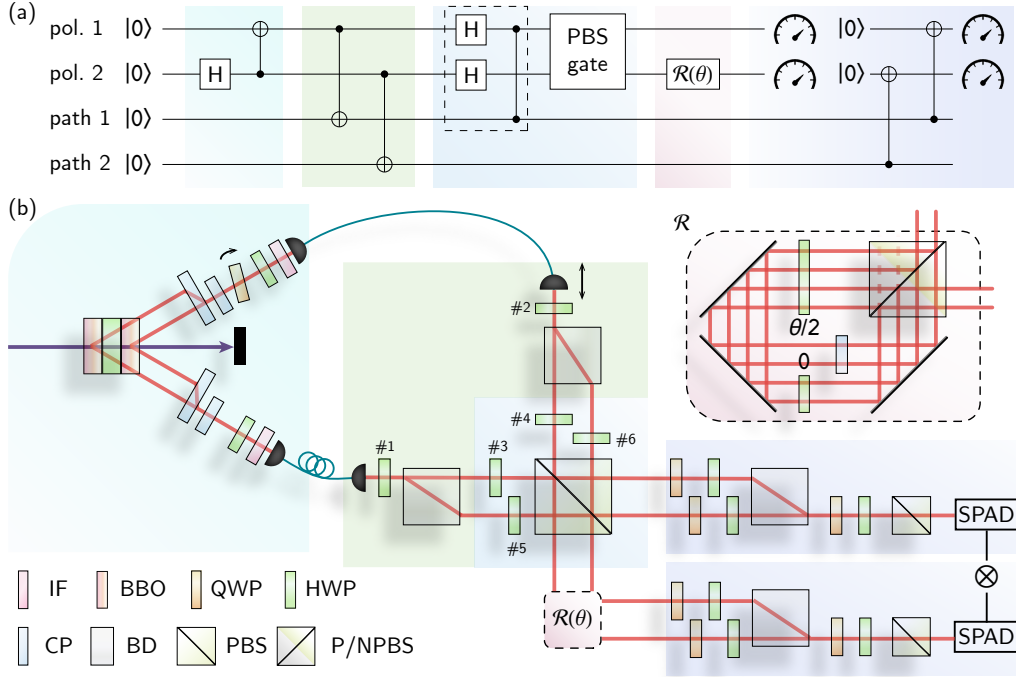
Fig. 2. **Experimental setup.** (a) The quantum circuit for generation and measurement of the 4-qubit linear cluster state $|LC_4(\theta)\rangle$ and GHZ state $|GHZ_4(\theta)\rangle$ using the polarization (pol.) and path degrees of freedom of a photon pair. The gates in the dashed box are only implemented when generating the $|LC_4(\theta)\rangle$. (b) The photonic realization of the quantum circuit. Aqua: the photon source, an ultraviolet pulsed laser pumps a sandwich β-barium borate (BBO) to generate two polarization entangled photons after spatial and temporal compensation. Green: state preparation. Two photons are further encoded into polarization and path modes. Navy blue: the PBS gate. Magenta: proposed nonunitary qubit rotation, capable of preparing the extended cluster/GHZ state $|LC_4(\theta)\rangle$, $|GHZ_4(\theta)\rangle$. Violet: joint measurements on polarization and path modes. IF interference filter, HWP half-wave plate, QWP quarter-wave plate, CP temporal/spatial compensation crystal, BD beam displacer, PBS polarizing beam splitter and P/NPBS a special beam splitter, with half of it coated as a PBS and the other half coated as a non-polarizing beam splitter.

The results for GHZ-type paradox observation via the perfect Hardy-type paradox observation (equation (7)) are plotted in Fig. 3. The probabilities of observing event correlations contrary to the LHV predictions for $|LC_4(0)\rangle$ $|GHZ_4(0)\rangle$, and $|GHZ_4(\pi/4)\rangle$ were $90.1\%, 94.4\%$, and 96.2%, respectively. To statistically refute the LHV models, we notice that each of the investigated Hardy-type paradoxes effectively contains four contradictory predictions, and the error rate of each measurement must be lower than $1/4$ to violate the Bell's inequality (4). The calculated detection probabilities are provided in the subplots of Fig. 3. All of the probabilities fall well into the statistically significant region (≥ 0.75 for all and ≤ 0.25 for nothing) by at least $56.0, 72.7$, and 93.9 standard deviations, corresponding to the GHZ-type paradox for $|LC_4(0)\rangle$ $|GHZ_4(0)\rangle$, and $|GHZ_4(\pi/4)\rangle$, respectively. Here, the errors are calculated by assuming a Poisson distribution for counting statistics and resampling over recorded data. The residual experimental error is mainly due to the instability of the Mach-Zehnder interferometer, and the non-unity visibility of two-photon interference. Taking experimental imprecision into account, our results reasonably satisfy required constraints and achieve high probability of successful observation of

nonclassical behaviors in the manner of a Hardy-type paradox.

Next, from the data for $|GHZ_4(0)\rangle$, we kept only the events that register a result of $+1$ on the σ_x measurement of the first qubit to prepare a $|GHZ_3\rangle$ state. Under this postselection, the remaining three qubits still exhibited the GHZ-type paradox in equation (1); this manifestation can be employed to demonstrate the applications of quantum state verification and entanglement detection. The observed GHZ paradox precludes another possible form of genuine three-qubit entanglement, namely, the W-state [45]. By giving a value of $\mathcal{I}_3 = 3.792$, our experimentally prepared three-qubit state shows a fidelity of at least 89.6% compared with the theoretical three-qubit GHZ state.

To experimentally test the steering paradox, we note that the classical prediction holds because the conditional density matrices for Bob are pure [29]. Consequently, we need to estimate the lower bound for the dominant eigenvalue of Bob's unnormalized conditional density matrix, and here the entanglement detection methodology can again play a role. Experimentally, Bob was instructed to jointly measure $\sigma_y \otimes \sigma_x$ and $\sigma_x \otimes \sigma_y$ on his two qubits when Alice measured $\sigma_y \otimes \sigma_x$ on her

qubits, and jointly measure $\sigma_x \otimes \sigma_x$ and $\sigma_y \otimes \sigma_y$ of his two qubits when Alice measured $\sigma_z \otimes \sigma_z$ on her qubits. Because the spectra of $\sigma_x \otimes \sigma_y + \sigma_y \otimes \sigma_x$ and $\sigma_x \otimes \sigma_x + \sigma_y \otimes \sigma_y$ are both $\{2, 0, 0, -2\}$, the expectation value of $\langle \sigma_x \otimes \sigma_y + \sigma_y \otimes \sigma_x \rangle$ and $\langle \sigma_x \otimes \sigma_x + \sigma_y \otimes \sigma_y \rangle$ for the conditional states can be exploited as a lower bound for the largest eigenvalue of the unnormalized conditional density matrix. This lower bound is further utilized to calculate the quantum value of $\mathcal{I}_s$ and experimentally reject the LHS prediction [29]. The calculated quantum value of $\mathcal{I}_s$ is 1.805 ± 0.014, which violates the prediction of the LHS model by 59 standard deviations, thus manifesting the nonclassical phenomenon of EPR steering.

III. DISCUSSION

This work advanced the study of the GHZ-type paradox in and beyond graph states. In Theorem 1, we present a unified construction of the GHZ-type paradox that naturally includes previous results for graph states. The paradox, when transformed into the Bell-type inequality, becomes an entanglement witness with a significantly lower threshold for refuting the separable models. These Bell-type inequality can also be exploited to estimate the fidelity between a quantum state and a target graph state, hence providing a promising way of eval-
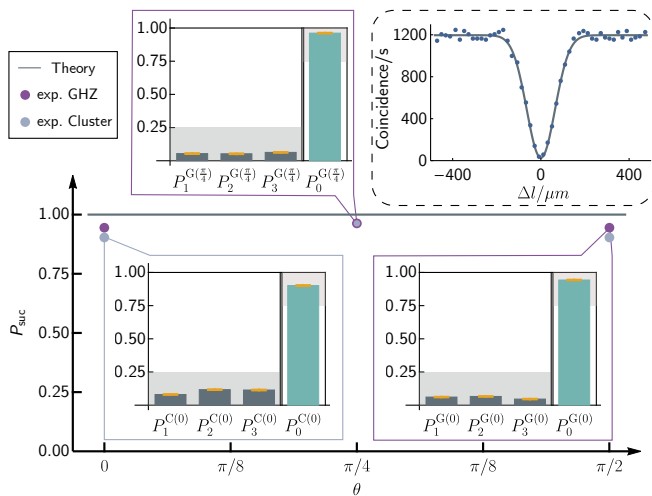

Fig. 3. **Experimental observation of the perfect Hardy-type paradox.** Data points: Calculated success probabilities that eventuate in Hardy-type paradox plotted against the state parameter θ. The error bars correspond to 1σ standard deviation. Gray points are for generalized cluster states and purple ones for GHZ states. Subplots: The sharp contradiction between LHV models and quantum theory corresponding to the Hardy constraints for given data points. Shaded areas represent the effective region of 75% visibility threshold. Dashed box: the Hong-Ou-Mandel dip of two photon interference (visibility $= 0.971$) and the Gaussian fitted curve. Each measurement result is recorded across a 30 second time span with the pumping power set to 20mW.
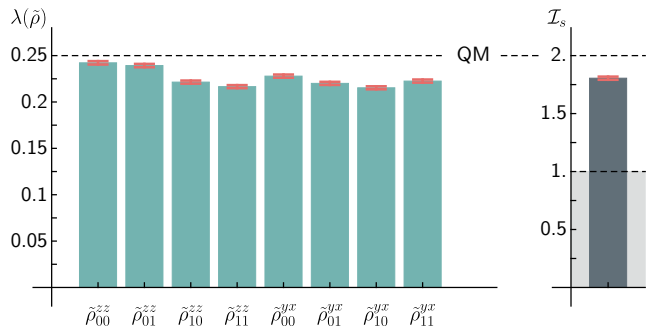

Fig. 4. **Experimental observation of the Hardy-type steering paradox.** Left: calculated maximum eigenvalues for Bob's marginal states of the mixed state (6), conditioned on Alice's possible measurement settings and results. Right: visualized quantum violation of $\mathcal{I}_s$ against the LHS prediction $\mathcal{I}_s = 1$. The error bars in both subplots correspond to 1σ standard deviation.

uating the capacity of a quantum state in specific tasks such as quantum error correction [46, 47] and magic state distillation [48].

Along with the Hamiltonian approach, we found that the GHZ-type paradox also exists in non-graph states. On one hand, a family of non-graph states and mixed states that also exhibits the GHZ-type paradoxes. This observation suggests that even mixed states can serve as resources for tasks like quantum pseudo-telepathy [49] and $l2$ measurement-based quantum computation [50], each of which typically requires highly-entangled pure states. On the other hand, the non-graph mixed states $\rho(\theta)$ can also be used for demonstrating the steering paradox $1_C = 2_Q$. We hence enriched quantum paradoxes for more kinds of quantum nonlocality. Since the nonclassical event occurs ideally in every round of experiment, our method has the potential of detecting steering using very few copies of states.

We have experimentally tested the GHZ-type paradoxes for graph and non-graph states by measuring the success probability in Hardy's paradox under Hardy-type constraints. Thus, we provide a more efficient way to demonstrate the GHZ-type paradox by turning it into a Hardy-type one. Our methodology also sheds some new light on the construction of a genuine multipartite GHZ-type paradoxes. In SI [29] we show that the mathematical tool of local complementation [51, 52] further enlarges the scope of quantum state verification. In particular, this method of quantum state verification is applicable to all the five-qubit graph states; we plan to investigate this property in the near future.

IV. METHODS

Construction of GHZ-type paradoxes for graph states.— To formulate unified GHZ-type paradoxes for the graph states with at least one universal vertex, we

start from the following observation: when two unconnected vertices are both connected to a third vertex, a minus sign appears in the product of the three stabilizers for these vertices when they are spanned on the Pauli basis, since the product on the third vertex gives $\sigma_z\sigma_x\sigma_z = -\sigma_x$. This gives a sign difference between classical and quantum prediction.

A GHZ-type paradox arise when we choose some products of the stabilizing operators (modulo the minus signs before the Pauli matrices), such that for every vertex, any Pauli matrix appear even times, so the product of the classical expectations is $+1$, regardless of the specific values assigned for the observables; and the three-stabilizer structure appears odd times, so the product of the quantum expectations is -1. Additionally, to involve every vertex connected to the universal one in the GHZ-type paradox, they are required to subject to two-setting (instead of one-setting) measurements, so the paradox cannot be simply reproduced by a biseparable quantum state by setting the qubit on the $+1$-eigenstate of the one-setting measurement [30].

For clarity, here we explicitly demonstrate the construction on the case of $n =$ even; the construction for $n =$ odd is very similar. To exploit the constraint of two-setting measurement, an ansatz of operator choices can be conjectured as $\{S_1, (-1)^{a_i}S_1^{a_i}S_iS_{i+1}\}$, so that the first observable S_1 forces a σ_z measurement on every peripheral vertices, leaving only one of σ_x and σ_y to be measured. This in turn gives $a_{i-1} \oplus C_{i-1}^i = a_i \oplus C_i^{i+1}$ for $i = 3, 4, \cdots, n$, as can be deduced from the form of the ansatz. Finally, the product of the quantum predictions being -1 requires $\sum_{i=2}^n a_i =$ odd. Solving the logical equations for a_i yields the results in Theorem 1.

Experimetnal setup.— A 780nm mode-locked femtosecond laser pumped an 1mm-thick bismuth triborate (BiBO) crystal to prepare high-power ultraviolet beam, which further pumped two identical 1mm-thick, type-2 beamlike phase-matching [53] β-barium borate (BBO) crystals, clipping on one true-zero-order half-wave plate (HWP), to prepare bright entangled biphotons [54]. After spatial and temporal compensation, the down-converted wavefunctions from two pump processes were overlapped and the fidelity of prepared state with $|\Psi^+\rangle = (|HV\rangle + |VH\rangle)/\sqrt{2}$ is 0.991. Here, $|0\rangle^{\text{pol}} = |H\rangle$ and $|1\rangle^{\text{pol}} = |V\rangle$ indicate the horizontal and vertical polarization of the photon. After filtered by 3nm bandwidth interference filter, the photons were guided to the main setup by single-mode fibers (SMF), preceded and succeeded by one HWP respectively, to compensate polarization dispersion within the fiber.

In the central interference setup, the polarization states of photons were converted to $(|\Phi^+\rangle = |HH\rangle + |VV\rangle)/\sqrt{2}$ by HWP #1 and #2 set at 22.5°. Two beam displacers (BDs) detoured horizontal polarized photon wavefunctions to the upper ($|0\rangle^{\text{path}} = |u\rangle$ for up) path, approximately 3mm away from the original lower ($|1\rangle^{\text{path}} = |d\rangle$ for down) path occupied by vertical po-

larized photon wavefunctions. At this point, the two path qubits were appended to the polarization qubits, and the entire biphoton state is effectively a GHZ state $|GHZ_4(\theta = 0)\rangle = (|HHuu\rangle + |VVdd\rangle)/\sqrt{2}$. Further conversion to cluster state $|LC_4(\theta = 0)\rangle = (|HHuu\rangle + |HHdd\rangle + |VVuu\rangle - |VVdd\rangle)/2$ was done by adjusting the orientations of HWP #3 $\sim$ #6 and exploiting the PBS gate, and the exact settings are given in SI [29].

To make joint path-polarization measurement, another pair of BDs was introduced to combine the two paths again and form a Mach-Zehnder intereferometer. Before each BD, two groups of polarization controllers, each containing a quarter-wave plate (QWP) succeeded by a HWP, were utilized to analyze state of polarization in each path. By carefully tilting the BDs, we compensated for the relative phase difference between the four possible paths. After the convergence of the displaced beams, another group of polarization controllers, together with a PBS, were used to measure the path state of each photon. The single-photon avalanche detectors were exploited to record coincidence counting rates. The length of the two Mach-Zehnder interferometers in the experimental setup was about 27.5cm. The integration time was 20s for each data point, giving about 10^4 possible counts for each state.

The non-unitary $\mathcal{R}(\theta)$ gate is required for the realization of variable θ. A Sagnac ring interferometer in the dashed box in Fig. 2 is sufficient for such operation, which was omitted in the actual experiment. The HWP at $\theta/2$ rotates the photon polarization, meanwhile, the HWP at 0° operating only on the counter-clockwise cycle of the ring provides the non-unitarity. Adding temporal compensation guarantees coherent superposition of the output beam. Nevertheless, by introducing a compensating HWP to flip the polarization state of a photon, the $\theta = \pi/4$ case was also experimentally realized.

The PBS gate and its benchmarking.— To illustrate the mechanism of the PBS gate, it is most intuitive to work in the second quantization picture. Let $\alpha_{\mu\nu}^\dagger$ denote the creation operator of the first photon on polarization mode μ and path mode ν, and $\beta_{\mu\nu}^\dagger$ denote which of the second photon. Further, let $\gamma_{\mu\nu}^\dagger$ and $\delta_{\mu\nu}^\dagger$ denote the creation operators of the photon that exits the PBS gate and propagates downward and rightward, respectively (cf. Fig. 2(b)). Under this notation, the mode conversion happening on the PBS gate can be expressed as $\alpha_{H\nu}^\dagger \to \gamma_{H\nu}^\dagger, \alpha_{V\nu}^\dagger \to i\delta_{V\nu}^\dagger, \beta_{H\nu}^\dagger \to \delta_{H\nu}^\dagger$, and $\beta_{V\nu}^\dagger \to i\gamma_{V\nu}^\dagger$. When the angles of the wave plates #3 $\sim$ #6 are set to $\theta_3/2 \sim \theta_6/2$, the inbounding wavefunction on the PBS gate is $\frac{1}{\sqrt{2}}[(\cos\theta_3\alpha_{Hu}^\dagger + \sin\theta_3\alpha_{Vu}^\dagger)(\cos\theta_4\beta_{Hu}^\dagger + \sin\theta_4\beta_{Vu}^\dagger) + (-\sin\theta_5\alpha_{Hd}^\dagger + \cos\theta_5\alpha_{Vd}^\dagger)(-\sin\theta_6\beta_{Hd}^\dagger + \cos\theta_6\beta_{Vd}^\dagger)]$. Using the mode conversion, the outbounding modes are $\frac{1}{\sqrt{2}}[(\cos\theta_3\gamma_{Hu}^\dagger + i\sin\theta_3\delta_{Vu}^\dagger)(\cos\theta_4\delta_{Hu}^\dagger + i\sin\theta_4\gamma_{Vu}^\dagger) + (-\sin\theta_5\gamma_{Hd}^\dagger + i\cos\theta_5\delta_{Vd}^\dagger)(-\sin\theta_6\delta_{Hd}^\dagger + \cos\theta_6 i\gamma_{Vd}^\dagger)]$. However, only the terms with both γ and δ operators result in coincident counting, so the final wavefunction

reads $\frac{1}{\sqrt{2}}[(\cos\theta_3\cos\theta_4\gamma_{Hu}^\dagger\delta_{Hu}^\dagger - \sin\theta_3\sin\theta_4\gamma_{Vu}^\dagger\delta_{Vu}^\dagger) + (\sin\theta_5\sin\theta_6\gamma_{Hd}^\dagger\delta_{Hd}^\dagger - \cos\theta_5\cos\theta_6\gamma_{Vd}^\dagger\delta_{Vd}^\dagger)]$. Thus, we can effectively generate the desired states by adjusting the orientations of the wave plates.

The PBS gate works ideally when the wavefunctions of the two incident photons are overlapped both spatially and temporally. However, due to the intrinsic difference between wavepackets of the two photons produced in type-II down-conversion [55], spectral filter and intrinsic dispersion from SMF are not enough to render them identical. To synchronize the arrival time of the two photons and characterize their indistinguishability, we exploit the HOM interference [43]. Explicitly, we rotated the polarization states of both photons to $|D\rangle = (|H\rangle + |V\rangle)/\sqrt{2}$ after they had passed through the first pair of BDs, measured the two polarizations on $|DA\rangle$ basis at the final detection, where $|A\rangle = (|H\rangle - |V\rangle)/\sqrt{2}$, and projected both of the path qubits on $|u\rangle$. By tuning the length of the delay line, we can scan the HOM curve as is presented in the inset of Fig. 3.

Data availability
The data that support the findings of this study are available from the authors upon request.

Competing interests
The authors declare no competing interests.

Author contributions
J.L.C. constructed the theoretical scheme. J.S.X. and Z.H.L designed the experiment. Z.H.L. performed the experiment with the help from M.Y., Q.L., Y.M., and K.S., whereas J.Z., Z.H.L., and H.X.M. contributed to the theoretical analysis. J.L.C. and H.Y.S. supervised the theoretical part of the project, J.S.X., C.F.L., and G.C.G. supervised the project. All authors read the paper and discussed the results.

Z.H.L and J.Z. contributed equally to this work.

[1] A. Einstein, B. Podolsky, and N. Rosen, Can Quantum-Mechanical Description of Physical Reality Be Considered Complete? Phys. Rev 47, 777 (1935).

[2] J. S. Bell, On the Einstein Podolsky Rosen paradox. Physics 1, 195 (1964).

[3] M. A. Nielsen, and I. L. Chuang, Quantum computation and quantum information (Cambridge universtiy press, Cambridge, UK, 2000).

[4] R. Raussendorf and H. J. Briegel, A One-Way Quantum Computer, Phys. Rev. Lett. 86, 5188 (2001).

[5] P. Walther, K. J. Resch, T. Rudolph, E. Schenck, H. Weinfurter, V. Vedral, M. Aspelmeyer and A. Zeilinger, Experimental one-way quantum computing, Nature 434, 169-176 (2005).

[6] A. K. Ekert, Quantum cryptography based on Bell's theorem. Phys. Rev. Lett. 67, 661 (1991).

[7] L. M. Duan, M. D. Lukin, J. I. Cirac and P. Zoller, Long-distance quantum communication with atomic ensembles and linear optics, Nature 414, 413-418 (2001).

[8] U. Vazirani, T. Vidick, Fully device independent quantum key distribution, Phys. Rev. Lett. 113, 140501 (2014).

[9] S. Pironio et al., Random numbers certified by Bell's theorem. Nature 464, 1021-1024 (2010).

[10] X. Ma, X. Yuan, Z. Cao, B. Qi and Z. Zhang, Quantum random number generation, npj Quantum Inf 2, 16021 (2016).

[11] N. Brunner, D. Cavalcanti, S. Pironio, V. Scarani, and S. Wehner, Bell nonlocality. Rev. Mod. Phys. 86, 419 (2014).

[12] E. Chitambar, and G. Gour, Quantum resource theories. Rev. Mod. Phys. 91, 025001 (2019).

[13] J. F. Clauser, M. A. Horne, A. Shimony, and R. A. Holt, Proposed Experiment to Test Local Hidden-Variable Theories, Phys. Rev. Lett. 23, 880 (1969).

[14] N. D. Mermin, Extreme Quantum Entanglement in a Superposition of Macroscopically Distinct States, Phys. Rev. Lett. 65, 1838 (1990).

[15] M. Ardehali, Bell inequalities with a magnitude of violation that grows exponentially with the number of particles, Phys. Rev. A, 46, 5375 (1992).

[16] A. V. Belinskiĭ and D. N. Klyshko, Interference of light and Bell's theorem, Phys. Usp. 36, 653 (1993).

[17] S. Abramsky and A. Brandenburger, The sheaf-theoretic structure of non-locality and contextuality, New J. Phys. 13, 113036 (2011).

[18] D. M. Greenberger, M. A. Horne, and A. Zeilinger, arXiv preprint 0712.0921. in Bell's Theorem, Quantum The-

ory, and Conceptions of the Universe, M. Kafatos (Ed.), Kluwer, Dordrecht, 69-72 (1989).

[19] L. Hardy, Nonlocality for two particles without inequalities for almost all entangled states, Phys. Rev. Lett. **71**, 1665 (1993).

[20] D. Boschi, S. Branca, F. De Martini, and L. Hardy, Ladder Proof of Nonlocality without Inequalities: Theoretical and Experimental Results, Phys. Rev. Lett. **79**, 2755 (1997).

[21] S. H. Jiang, Z. P. Xu, H. Y. Su, A. K. Pati, and J. L. Chen, Generalized Hardy's Paradox, Phys. Rev. Lett. **120**, 050403 (2018).

[22] J. L. Chen, A. Cabello, Z. P. Xu, H. Y. Su, C. Wu, and L. C. Kwek, Hardy's paradox for high-dimensional systems, Phys. Rev. A **88**, 062116 (2013).

[23] J. W. Pan, D. Bouwmeester, M. Daniell, H. Weinfurter, A. Zeilinger, Experimental test of quantum nonlocality in three-photon Greenberger–Horne–Zeilinger entanglement. Nature (London) **403**, 515 (2000).

[24] D. L. Deng, C. Wu, J. L. Chen, and C. H. Oh, Fault-Tolerant Greenberger-Horne-Zeilinger Paradox Based on Non-Abelian Anyons, Phys. Rev. Lett. **105**, 060402 (2010).

[25] V. Scarani, A. Acín, E. Schenck, and M. Aspelmeyer, Nonlocality of cluster states of qubits, Phys. Rev. A **71**, 042325 (2005).

[26] W. Tang, S. Yu, and C. H. Oh, Greenberger–Horne–Zeilinger Paradoxes from Qudit Graph States, Phys. Rev. Lett. **110**, 100403 (2013)

[27] H. M. Wiseman, S. J. Jones, and A. C. Doherty, Steering, Entanglement, Nonlocality, and the Einstein–Podolsky–Rosen Paradox, Phys. Rev. Lett. **98**, 140402 (2007).

[28] H. J. Briegel and R. Raussendorf, Persistent Entanglement in Arrays of Interacting Particles, Phys. Rev. Lett. **86**, 910 (2001).

[29] See Supplementary Information for proofs of the theorem, some examples and experimental details.

[30] O. Gühne, G. Tóth, P. Hyllus, and H. J. Briegel, Bell Inequalities for Graph States, Phys. Rev. Lett. **95**, 120405 (2005).

[31] G. Tóth, O. Gühne, and H. J. Briegel, Two-setting Bell inequalities for graph states, Phys. Rev. A **73**, 022303 (2006)

[32] A. Cabello, O. Gühne, and D. Rodríguez, Mermin inequalities for perfect correlations, Phys. Rev. A **77**, 062106 (2008)

[33] J. Eisert and H. J. Briegel, Schmidt measure as a tool for quantifying multiparticle entanglement, Phys. Rev. A **64**, 022306 (2001).

[34] S. Yu, Q. Chen, C. Zhang, C. H. Lai, and C. H. Oh, All Entangled Pure States Violate a Single Bell's Inequality Phys. Rev. Lett. **109**, 120402 (2012).

[35] J. L. Chen, H. Y. Su, Z. P. Xu, and A. K. Pati, Sharp Contradiction for Local-Hidden-State Model in Quantum Steering, Sci. Rep. **6**, 32075 (2016).

[36] M. Yang, H. X. Meng, J. Zhou, Z. P. Xu, Y. Xiao, K. Sun, J. L. Chen, J. S. Xu, C. F. Li, and G. C. Guo, Stronger Hardy-type paradox based on the Bell inequality and its experimental test Phys. Rev. A **99**, 032103 (2019).

[37] Z. P. Xu, J. L. Chen, and O. Gühne, Proof of the

Peres conjecture for contextuality, Phys. Rev. Lett. **124**, 230401 (2020).

[38] D. E. Browne and T. Rudolph, Resource-Efficient Linear Optical Quantum Computation, Phys. Rev. Lett. **95**, 010501 (2005).

[39] T. P. Bodiya and L. M. Duan, Scalable Generation of Graph-State Entanglement Through Realistic Linear Optics, Phys. Rev. Lett. **97**, 143601 (2006).

[40] N. K. Langford, T. J. Weinhold, R. Prevedel, K. J. Resch, A. Gilchrist, J. L. O'Brien, G. J. Pryde, and A. G. White, Demonstration of a Simple Entangling Optical Gate and Its Use in Bell-State Analysis, Phys. Rev. Lett. **95**, 210504 (2005).

[41] G. Vallone, E. Pomarico, P. Mataloni, F. De Martini, and V. Berardi, Realization and Characterization of a Two-Photon Four-Qubit Linear Cluster State, Phys. Rev. Lett. **98**, 180502 (2007).

[42] W. H. Zhang, G. Chen, P. Yin, X. X. Peng, X. M. Hu, Z. B. Hou, Z. Y. Zhou, S. Yu, X. J. Ye, Z. Q. Zhou, X. Y. Xu, J. S. Tang, J. S. Xu, Y. J. Han, B. H. Liu, C. F. Li and G. C, Guo, Experimental demonstration of robust self-testing for bipartite entangled states, npj Quantum Inf. **5**, 4 (2019).

[43] C. K. Hong, Z. Y. Ou, and L. Mandel, Measurement of subpicosecond time intervals between two photons by interference, Phys. Rev. Lett. **59**, 2044 (1987).

[44] L. C. Ryff, Bell and Greenberger, Horne, and Zeilinger theorems revisited, Am. J. Phys, **65**, 1197 (1997).

[45] W. Dür, G. Vidal, and J. I. Cirac, Three qubits can be entangled in two inequivalent ways, Phys. Rev. A **62**, 062314 (2000).

[46] B. A. Bell, D. A. Herrera-Martí, M. S. Tame, D. Markham, W. J. Wadsworth, and J. G. Rarity, Experimental demonstration of graph-state quantum secret sharing, Nat. Commun. **5**, 3658 (2014).

[47] D. Gottesman, Quantum fault tolerance in small experiments, arXiv: 1610.03507 (2016).

[48] S. Bravyi and A. Kitaev, Universal quantum computation with ideal Clifford gates and noisy ancillas, Phys. Rev. A **71**, 022316 (2005).

[49] G. Brassard, A. Broadbent, and A. Tapp, Multi-party pseudo-telepathy, in *Workshop on Algorithms and Data Structures*. Springer, Berlin, Heidelberg, pp. 1-11 (2003).

[50] R. Raussendorf, Contextuality in measurement-based quantum computation, Phys. Rev. A **88**, 022322 (2013).

[51] M. Hein, J. Eisert, and H. J. Briegel, Multiparty entanglement in graph states, Phys. Rev. A **69**, 062311 (2004).

[52] J. C. Adcock, S. Morley-Short, A. Dahlberg, and J. W. Silverstone, Mapping graph state orbits under local complementation, Quantum **4**, 305 (2020).

[53] C. Kurtsiefer, M. Oberparleiter, and H. Weinfurter, Generation of correlated photon pairs in type-II parametric down conversion, J. Mod. Opt. **48**, 1997 (2001).

[54] C. Zhang, Y. F. Huang, Z, Wang, B. H. Liu, C. F. Li, and G. C. Guo, Experimental Greenberger–Horne–Zeilinger-Type Six-Photon Quantum Nonlocality, Phys. Rev. Lett. **115**, 260402 (2015).

[55] Y. Shih, *An Introduction to Quantum Optics: Photon and Biphoton Physics*, Taylor & Francis, 2014.